RSC Advances

PAPER

View Article Online
View Journal | View Issue

Cite this: *RSC Adv.*, 2025, **15**, 3979

Dendritic fibrous nanosilica activated bovine excrement fiber to enhance the initial characteristics and durability of concrete

Mohsen Karimi,[a] Seyed Mojtaba Movahedifar,*[a] Amin Honarbakhsh,*[ab] Mahdi Nobahari[a] and Rahele Zhiani[cde]

The global agricultural sector has persistently grappled with the effective handling of bovine waste. This research repurposes bovine waste into a cost-effective and sustainable fiber, which is subsequently treated with dendritic fibrous nanosilica (DFNS) to produce CDF/DFNS. This is then integrated into cement-based composites. This study aimed to introduce CDF/DFNS to enhance the operational efficiency and longevity of Portland cement with notable sulfate resistance. Concurrently, CDF/DFNS was incorporated into cement mortar, and an examination of the aggregation of CDF/DFNS, along with the aquation procedure and microstructure of the mortar, was conducted. The investigation indicated that incorporating CDF/DFNS enhanced the toughness, tangible attributes, and imperishability of the cement specimens. The integration of CDF/DFNS resulted in a reduction in both the parameters related to the movement of chloride ions and the volume of voids in a material. Furthermore, the ability of cement mortar to resist compression forces was improved with the presence of CDF/DFNS as opposed to control samples. These improvements in strength and imperishability suggested that CDF/DFNS holds significant potential in reducing CO_2 emissions in the concrete industry.

Received 6th August 2024
Accepted 27th January 2025

DOI: 10.1039/d4ra05716c

rsc.li/rsc-advances

Introduction

Effectively repurposing bovine excrement waste into novel construction materials is a hopeful and environmentally sound resolution for the building industry.[1–8] Bovine excrement could be processed into solid fibre, known as Cow Dung Fibre (CDF), which is an organic lignocellulose-based fibre primarily comprised of cellulose, hemi-cellulose, and lignin.[9–14] Unlike artificial filaments such as carbon fibre, basalt fibre, and glass fibre, organic filaments like CDF offer advantages such as being lightweight, cost-effective, biodegradable, and renewable, making them highly suitable for reinforcing cement-based materials.[15–18] Studies have demonstrated that integrating organic filaments into cement-based composites could notably enhance their compressive strength, bendability, and tenacity.[19] Nonetheless, addressing the suitability of organic filaments and cement-based structures remains an outstanding challenge.[20]

Marine concrete, a material widely used in coastal emerging countries, is known for its inherent tangible characteristics and imperishability.[21] It is important to note that the production of cement, which accounts for 8% of global carbon emissions, is profoundly influenced by the pervasive use of concrete, leading to a notable expulsion of CO_2. Furthermore, the use of concrete is impeded by the harmful effects of deterioration caused by SO_4^{2-} and Cl^- in the harsh marine environment. A number of research studies[22–24] have underscored the difficulties presented by this degradation. An alternative approach to addressing this concern is to improve the strength and imperishability of concrete, which could result in a decrease in cement usage and a rise in the lifespan of the concrete architecture.[25–28] In doing this, the release of carbon dioxide can be substantially diminished.[29] Chloride-induced reinforcement deterioration in concrete structures adversely affects its imperishability. In other words, it results in a reduction of life expectancy, a pressing matter that requires immediate attention.

In this study, CDF underwent pretreatment with a NaOH solution, followed by activation with DFNS, and ultimately incorporation into cement-based composites. The research delved into the impact of varying intensities of NaOH blend and immersing durations on the bulk reduction of CDF, seeking to aid the successful utilization of CDF in cement-based composites. Various analyses, including TGA, FTIR, and SEM, were conducted to investigate the alterations in the primary compounds of CDF/DFNS. The physical characteristics and auto-generated contraction of the cement-based mixtures

[a]*Department of Civil Engineering, Islamic Azad University, Neyshabur Branch, Neyshabur, Iran. E-mail: movahedi_far@yahoo.ca; amin_honarbakhsh@yahoo.com*
[b]*New Materials Technology and Processing Research Center, Department of Civil Engineering, Islamic Azad University, Neyshabur Branch, Neyshabur, Iran*
[c]*Department of Chemistry, Islamic Azad University, Neyshabur Branch, Neyshabur, Iran*
[d]*New Materials Technology and Processing Research Center, Department of Chemistry, Islamic Azad University, Neyshabur Branch, Neyshabur, Iran*
[e]*Advanced Research Center for Chemistry, Biochemistry and Nanomaterial, Islamic Azad University, Neyshabur Branch, Neyshabur, Iran*

Table 1 Primary chemical makeup of slag and cement by weight

	MgO	Al_2O_3	MnO	CaO	Fe_2O_3	SO_3	Na_2O	SiO_2	K_2O	TiO_2
Cement	3.01	4.70	0.18	53.24	4.11	4.47	0.32	26.11	0.33	3.01
Slag	8.08	12.90	0.35	46.90	0.74	2.48	0.32	22.10	0.36	0.89

Table 2 Characteristics of the sands' physical properties

Apparent density (kg m^{-3})	Specific density (kg m^{-3})	Fineness module	Clay content (%)	Particle size (mm)
1450	2500	2.5	<0.15	<5.00

containing CDF/DFNS were assessed, while the influx of NaOH mixture pre-soaking on CDF was also scrutinized.[30]

Experimental section

Materials

In this research, we utilized ordinary Portland cement PO 52.5 produced by Fars Cement Company, Iran. The primary chemical makeup of the cement and slag were identified through X-ray fluorescence and are detailed in Table 1. Standard sands were employed as the fine aggregates, and Table 2 presents the physical properties of these sands. The bovine excrement used in this study was sourced from the Farm of Neyshabur Technical and Vocational College in Neyshabur, Iran. The cows at this farm were primarily fed with alfalfa, resulting in a significant presence of fibrous plant material in the excrement. Recently excreted bovine excrement was routinely gathered and deposited in an underground sewage treatment tank for 7 days to undergo bacterial breakdown. Following the secondary fermentation, the excrements were subjected to a segregation process using typical water flow from a faucet, which facilitated the division of the liquid mixture of excrement and retention of the filaments. The utilization of hot water in this process would further aid in separating the fibre from the dung. Additionally, two to three layers of folded cotton fabric were employed to achieve this separation. The size distribution of the resulting CDF is detailed in Table 3.

Preparation of the CDF

The cow dung fibre underwent pretreatment with sodium hydroxide at various intensities (0.2, 0.5, 1.0, 1.5, and 2.0 mol L^{-1}) and was subjected to five different soaking durations (3, 6, 12, 24, and 36 hours). Following the soaking process, the CDF was thoroughly rinsed with distilled water until it reached a pH value of 7. Subsequently, the CDF was dried in an oven at 80 °C for 10 hours. The optimal intensity and length of time for sodium hydroxide blend pretreatment were specified on the basis of the assessment of the CDF's mass loss rate.

Table 3 Distribution of particle sizes in CDF

Sieve size (mm)	<10	<1.7	<1	<0.3	<0.08
Cumulative passing (%)	100	60	70	25	0

Preparation of the CDF-reinforced cement-based composites

The CDF underwent pretreatment using NaOH blends with intensities of 1, 1.5, and 2 mol L^{-1} for a duration of 24 hours. Three distinct binder systems were formulated. Type A consisted of plain cement excluding CDF. Type B comprised fibre-cement with a 2 wt% addition of CDF relative to the cement. Type C involved fibre-slag-cement with a 2 wt% addition of CDF/DFNS. The mixture ratios of mortar samples are detailed in Table 4, with the solution/binder (s/b) ratio maintained at 0.7. The CDF content was consistently set at 2 wt% of the binder. Both the waste sodium hydroxide blend after cow dung fibre pretreatment and deionized water were utilized as mixing blends for preparing the mortar cases. Their respective performances were assessed and then compared. It is noteworthy that the employment of the waste sodium hydroxide blend after cow dung fibre pretreatment for preparing the mortar cases held significance and helped prevent potential secondary pollution from waste alkali solutions.

Results and discussion

In this investigation, the first phase encompassed the creation of pre-treated CDF, following the methodologies outlined in the current body of work. These commodities were subsequently prepared for use by employing DFNS to co-immobilize CDF/DFNS onto the respective matrices (CDF). This process is schematically represented in Scheme 1.

Table 4 Mix features of cement-based mortars

Type	Sand (kg m^{-3})	Cement (kg m^{-3})	CDF (kg m^{-3})	Mixing solution (kg m^{-3})	Solution/binder
Type A	1300	500	0	220	0.7
Type B	1300	500	10	220	0.7
Type C	1300	500	10	220	0.7

The SEM micrographs in Fig. 1 reveal the surface morphology of CDF and CDF/DFNS. The raw fibre exhibited a relatively smooth, uniform, and glossy surface (Fig. 1a), whereas the surface texture became rough after the addition of DFNS (Fig. 1b). The FTIR analysis of CDF and CDF/DFNS, depicted in Fig. 2, revealed similar patterns of lignocellulose fibre, encompassing hemicellulose, lignin, and cellulose. A prominent imbibitions maximum typically appeared in the 3340 cm^{-1} range, attributed to the hydrogen bonding of cellulose. Additionally, noticeable absorption peaks between 2940 and 2880 cm^{-1} corresponded to the H–C stretching vibration of H–C–H and H–C in DFNS.

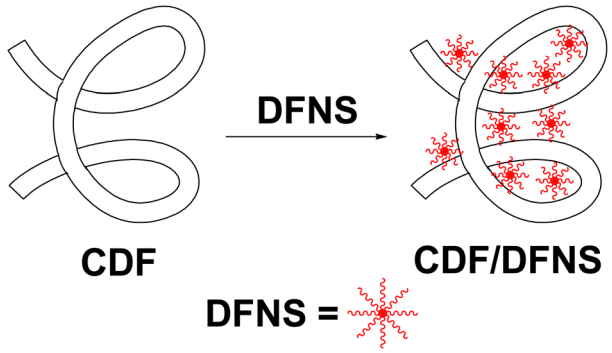

Scheme 1 Preparation process of CDF/DFNS.

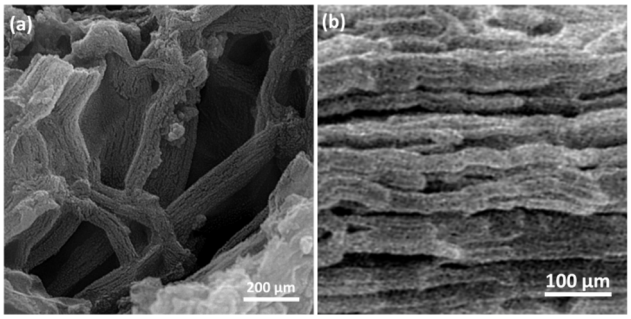

Fig. 1 SEM image of the (a) CDF and (b) CDF/DFNS.

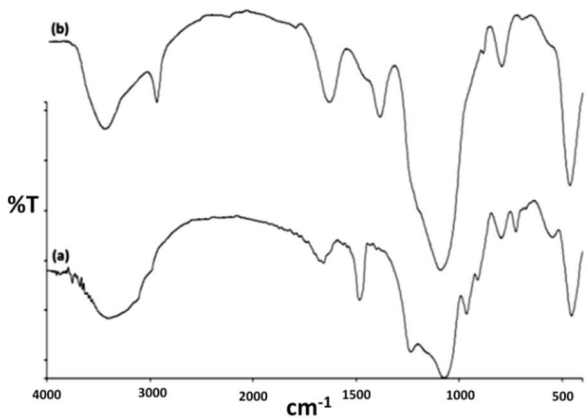

Fig. 2 FTIR spectra of (a) CDF, and (b) CDF/DFNS.

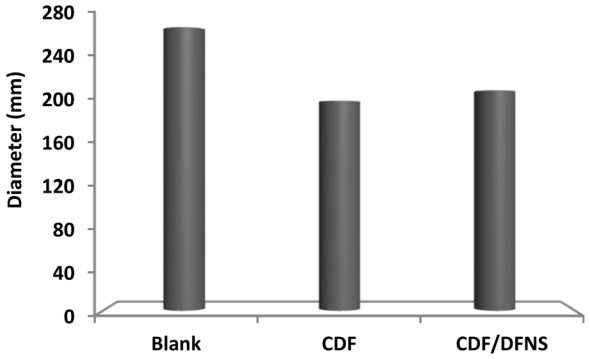

Fig. 3 Impact of CDF and CDF/DFNS on liquescence.

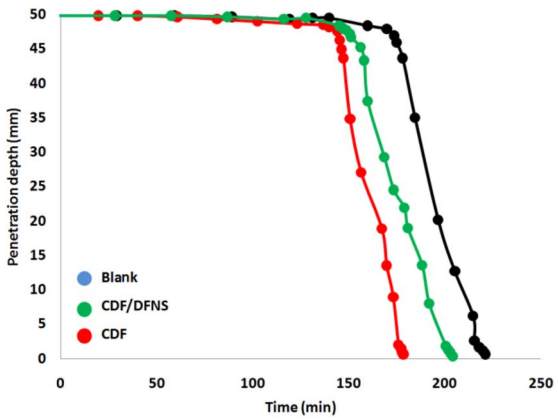

Fig. 4 The significance of CDF and CDF/DFNS in the timeframe of cement paste hardening.

The assessment of additives in cement-based mixtures was fundamentally based on their impact on workability, which is a fundamental measure. Fig. 3 focuses on the effect of CDF and CDF/DFNS on the liquescence and solidification period of cement. The findings from Fig. 4 showed that the liquescence of CDF and CDF/DFNS samples was significantly higher compared to the control samples. This implies that the DFNS grafting technique positively influenced the workability of CDF as admixtures. The inclusion of CDF and CDF/DFNS led to an increase during both the commencing and ultimate stages of the cement paste hardening process. The anticipated finding ties the accelerated cement solidification to the nucleation and pozzolanic effect of CDF/DFNS. Moreover, a higher grafting ratio intensified the delaying influence and the hindrance caused by the silane coupling agent in CDF and CDF/DFNS could also be influential.

The rheological properties of the cement paste, when CDF and CDF/DFNS were added, are depicted in Fig. 5. There is a positive linear interrelation between tangential shear and velocity gradient. The correlation is depicted by the lines that best fit the curves, adhering to the Bingham model. This is articulated in eqn (1). The Bingham model is frequently employed as a descriptor of the flow behavior of certain types of fluids, including cement paste. This model proposes that under conditions of low-velocity gradients, the fluid exhibits

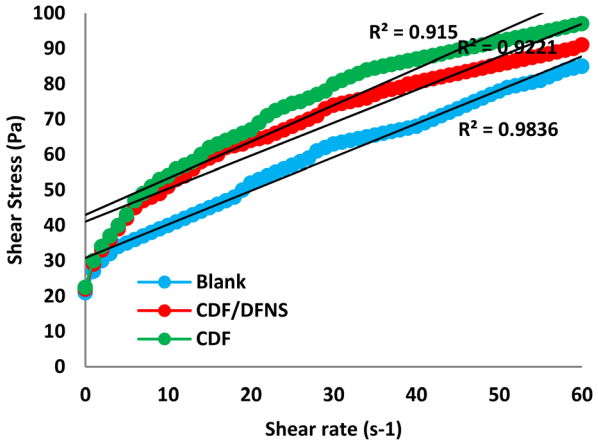

Fig. 5 Examination of the influence of CDF and CDF/DFNS on the dynamic tangential stress in cement paste.

characteristics akin to a rigid body. However, when subjected to high-velocity gradients, it transitions to behave more like a viscous fluid. This suggests a dual nature of the fluid's behavior dependent on the velocity gradient conditions. The positive linear correlation observed in this study indicates that the addition of CDF and CDF/DFNS enhanced the flow behavior of the cement paste, potentially improving its workability and performance.

$$\tau = \tau_o + \mu \frac{d\gamma}{dt} \quad (1)$$

τ = tangential stress, μ = plastic viscosity, τ_o = dynamic yield stress, $\frac{d\gamma}{dt}$= tangential rate.

The elastic limit significantly increased after the addition of CDF and CDF/DFNS (Fig. 6). This can be imputed to the large exteriors of the nanosilica particles in CDF and CDF/DFNS, which enhanced the uptake of water in the cement mixture. This uptake, subsequently, led to an increase in shear thickening in the paste. The grafting of DFNS groups onto the surfaces introduced a certain degree of hydrophilicity. An increase in the grafting rate led to an increase in hydrophilicity, which further increased the water absorption by CDF/DFNS and the shear force. As a result, as the grafting of DFNS intensified, the shear thickening became more noticeable. However, it was observed that the plastic viscosity showed minimal to no change under the influence of CDF and CDF/DFNS.

Fig. 7 shows the effect of CDF and CDF/DFNS on the elastic limit of the cement paste. The trend in the elastic limit of the three cement paste specimens was similar, as the elastic limit initially increased to attain a peak value, and then dropped to a steady state. Nevertheless, it is important to note that the peak value of the elastic limit varied among the seven cement pastes (see Fig. 8). This variation mirrored the pattern observed in the assessed yield stress shown in Fig. 9. This event might possibly be defined by changes in water adsorption due to hydrophilic chemical grafting and alterations in shear force.

Fig. 10 and 11 illustrate the impact of CDF and CDF/DFNS on the rate and total thermal energy release during the aquation

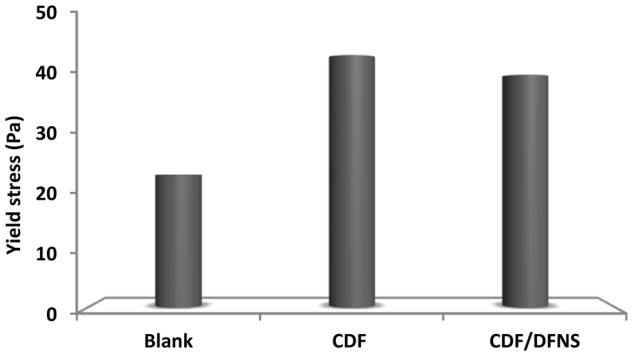

Fig. 6 Investigation into the impact of CDF and CDF/DFNS on the elastic limit of cement paste.

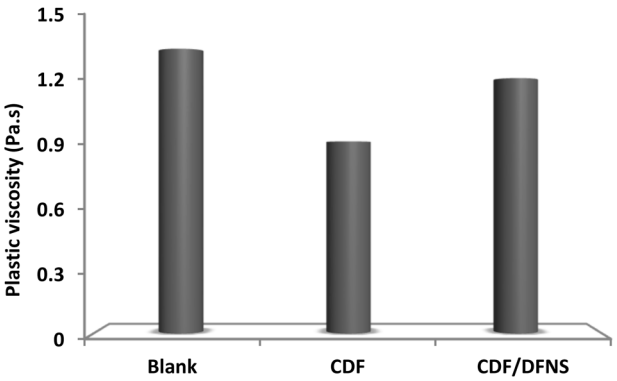

Fig. 7 Study of the effect of CDF and CDF/DFNS on the plastic viscosity of cement paste.

process of cement. As depicted in Fig. 11, the heat transfer efficiency graphs of the cement mixture, post the incorporation of CDF and CDF/DFNS, retained a similar form to that of the control case, without any extra peaks or alterations. However, changes were noted in the maximum strength and its occurrence. For example, the introduction of 2 weight percent CDF resulted in a change in the apex of heat emission from 10.6

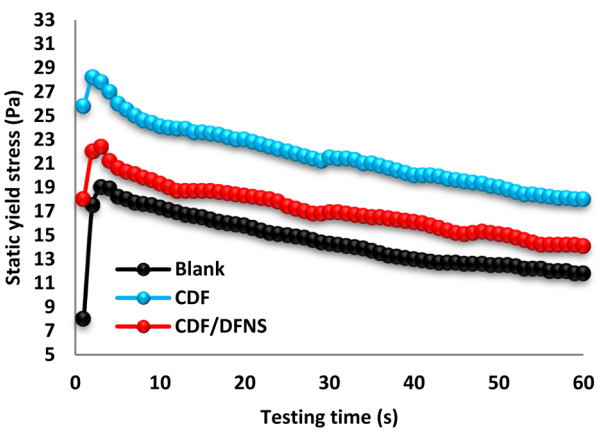

Fig. 8 Analysis of the role of CDF and CDF/DFNS in the elastic limit of cement paste.

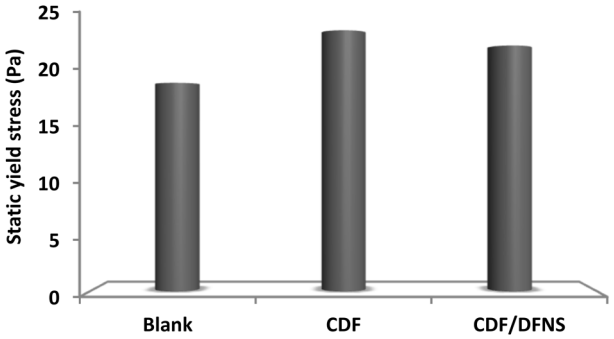

Fig. 9 Evaluation of the contribution of CDF and CDF/DFNS to the apex static efficacy strain of cement paste.

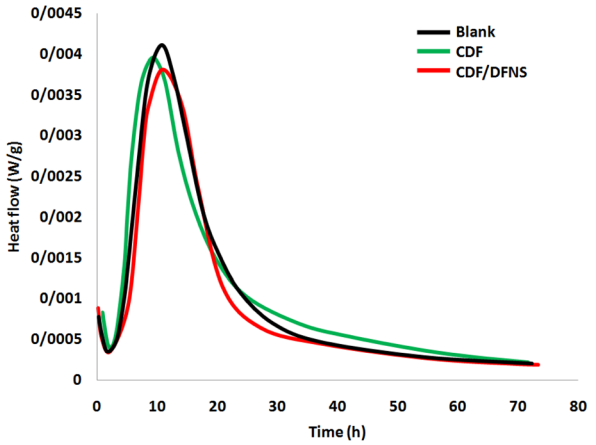

Fig. 10 The influence of CDF and CDF/DFNS on the thermal flow of cement paste.

hours to 8.3 hours. The amplifying effect on the cement hardening process can be imputed to CDF. With its substantial surface area and inherent intense reactivity as a pozzolan, CDF was able to rapidly interact with the moisturization offspring of cement. This interaction accelerated the disintegration tempo of cement particle, thereby enhancing the overall hardening process. When 2 percent by weight of CDF/DFNS was introduced, it resulted in an increase in the dissolution time of cement particles by 0.5 hours during the initial aquation phase (compared to the control paste). Although the existence of CDF/DFNS considerably hindered cement solidification, no noticeable changes were noticed in the rate of aquation product generation. Differing from the baseline scenario, the peak heat discharge of binder solidification was found to be postponed when deploying CDF and CDF/DFNS. This inference implied that the moment of the initial peak was progressively delayed as the grafting rate escalated, potentially due to the disturbance instigated by CDF/DFNS in the aquation reaction.

Fig. 11 illustrates the effect of CDF and CDF/DFNS on the total heat-releasing process of cement mixture. The slight increase in the entire heat-releasing process of the CDF cement could possibly be due to the accelerated reaction induced by CDF. At present, the mechanisms that govern the interaction

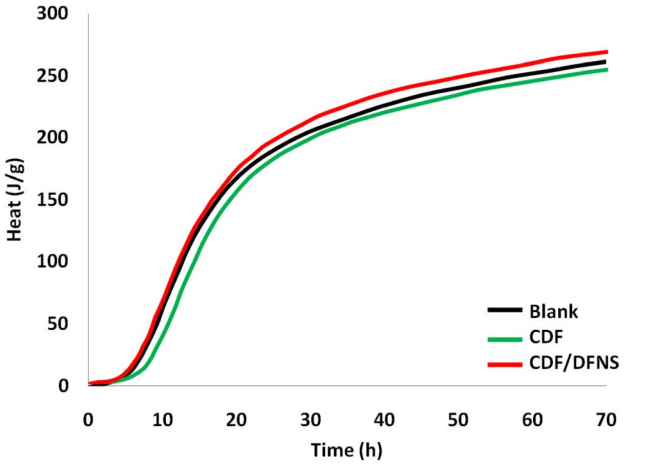

Fig. 11 The influence of blank, CDF, and CDF/DFNS on the cumulative heat of cement paste.

between CDF/DFNS and cement paste are not fully understood. It was also noted that the existence of DFNS led to a postponement of the cement solidification process, with different graft rates of DFNS resulting in varying thermal energy currents. In summary, the process by which CDF and CDF/DFNS affected cement solidification was largely dependent on the germination effect and pozzolanic reaction of CDF, which aided in the formation of aquation compounds. The existence of DFNS on the exterior of CDF/DFNS could potentially obstruct cement solidification. This was because the coating effect of the DFNS functional groups could potentially lead to a delay.

The XRD patterns of cement paste incorporating CDF and CDF/DFNS were analyzed over periods of 7, 14, and 21 days. The addition of CDF and CDF/DFNS had a minimal effect on the distinct stages that occur within a cement paste, which predominantly included belite, calcite, portlandite, ettringite, and alite. Compared to the reference cement samples, the intensity of the Ca–OH peak decreased in the cement with CDF, indicating a reduction in Ca–OH and the formation of H–S–C due to the pozzolanic reaction of colloidal silica nanoparticles. According to the Rietveld refinement analysis, the presence of CDF in the samples resulted in a substantial reduction in the proportion of Ca–OH by mass compared to the reference samples subsequent to a healing duration of 7 days (Table 5). This reduction can be ascribed to the aquation enhancement of CDF. In the same manner, following a healing duration of 7 days, the specimens incorporating CDF/DFNS were discovered to possess a diminished mass proportion of calcium hydroxide in comparison to the reference specimens. Nonetheless, this decrease was less noticeable than in the specimens incorporating CDF. This observation provided evidence for the beneficial effect of DFNS attachment in decreasing the pace of aquation in cement-CDF amalgams. Moreover, as the healing age increased, the peak values of aquation products, specifically H–O–Ca, showed a rising trajectory. This suggested that the inclusion of 2.1 wt% of CDF and CDF/DFNS had a trivial effect on the substances formed during the aquation reaction at a subsequent stage.

Table 5 Phase mass fraction of Ca–OH after Rietveld refinements

	Rehabilitating time		
Runs	7 days (%)	14 days (%)	21 days (%)
Blank	22.61	25.32	29.87
CDF	11.32	13.04	15.36
CDF/DFNS	11.91	13.03	16.59

Fig. 12 illustrates the role of CDF and CDF/DFNS in the pore structure of mortar after 21 days of healing. The pores observed in the thickened mortar comprised gel pores (measuring less than 0.03 μm) and capillary pores. Among these pores, there were medium ones spanning between 0.03 and 0.06 μm as well as large ones spanning between 0.06 and 9.8 μm. It is vital to highlight that the massive and medium ones had the most negative effect on the tangible attributes and resistance to chloride penetration of the mortar. This was predominantly owing to the condensation of voids happening in these kinds of pores. This led to a rise in the pressure and permeability of the capillary pores, which in turn decreased the concrete's resistance to fluid penetration. The inclusion of

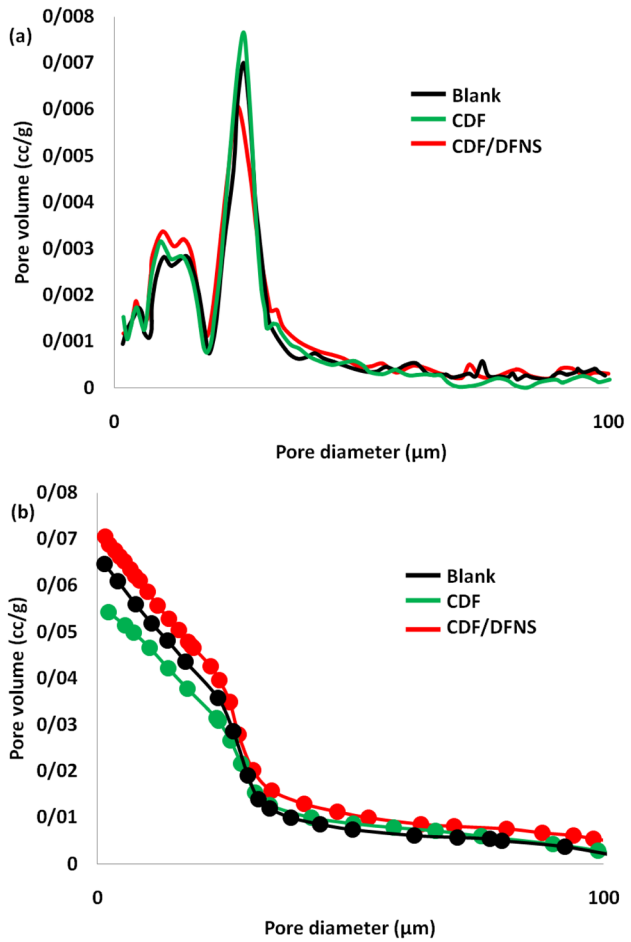

Fig. 12 The distribution of opening measurements (a), and cumulative opening volume of cement healed at 21 days >200 (b).

Table 6 Vent volumes of the different vents and cumulative vent volume

	Blank (%)	CDF (%)	CDF/DFNS (%)
<20 nm	3.528	3.817	4.401
20–100 nm	4.022	4.134	3.902
100–200 nm	0.536	0.417	0.539
>200 nm	2.024	1.715	1.203
Cumulative vent volume	15.381	15.267	13.057

CDF enhanced the architecture of mid-sized and large capillary pores within the hardened cement paste. This could be due to the formation of additional C–S–H between CDF and H–O–Ca, along with the pore-filling impact of this particle. Table 6 shows that the incorporation of DFNS–CDF led to the optimization of the pore architecture in the thickened mortar. Out of all, CDF/DFNS displayed the most significant effect of refinement on the pore structure, a phenomenon that can be related to its reduced link speed. The appropriate link speed of CDF/DFNS led to the generation of certain spatial stability and hydrophobicity. This guaranteed an even spread of CDF particles and had minimal impact on the viscosity of cement. Consequently, it ensured the thickness of the case and was anticipated to disrupt the chloride ion transport route. Fig. 13 shows the pore volumetric content of cement mortar samples. It is clear that the cases with 2.1 wt% of CDF/DFNS showed a marginally reduced proportion of detrimental pores (with diameters exceeding 100 nm) in comparison to the rest of the samples. This observation defined why the cases incorporating 2 wt% of CDF/DFNS demonstrated high strength in the subsequent zone.

Fig. 14 illustrates the influence of CDF/DFNS and CDF on the crushing and bending robustness of the cured mortar after 7, 14, and 21 days of curing. The bending robustness of the cement mortar with CDF additives was similar to that of the control cement mortar, while the flexural strength of the cement mortar with CDF/DFNS was superior to the control cement mortar. The addition of CDF and CDF/DFNS led to a significant augmentation in the crushing strength of the solidified cement paste, with the subsequent additives

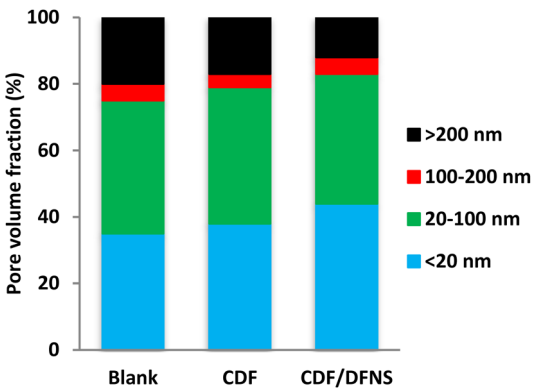

Fig. 13 Vent volume fraction of cement healed at 21 days.

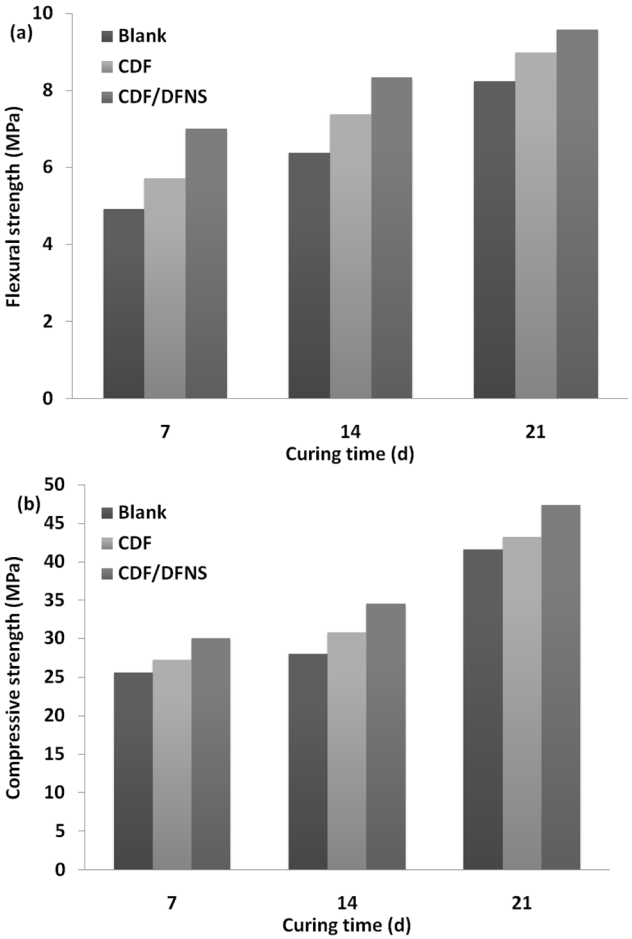

Fig. 14 Role of CDF and CDF/DFNS in (a) bending rigidity, (b) compressive force of cement at the recovery generation of 21 days.

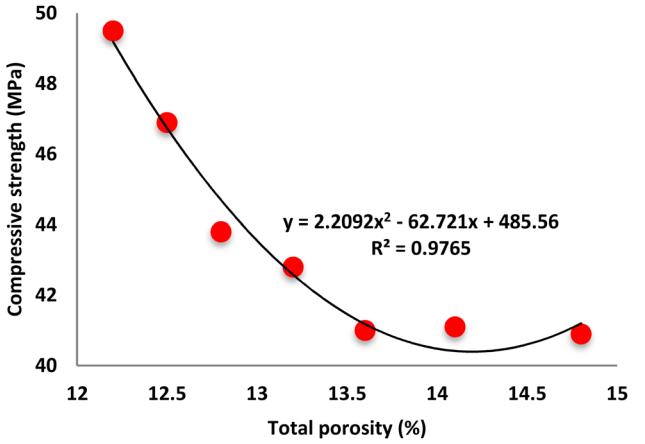

Fig. 15 Role of DFNS–CDF in the numerical correlation between total permeability and compressive intensity at the healing age of 21 days.

showing a more noticeable intensification. The high pozzolanic behaviour of CDF in DFNS–CDF can be credited to its capability to enhance the aquation process of cement. Additionally, it efficiently soaks up the calcium hydroxide that was abundant in the Interfacial Transition Zone (ITZ) situated between the composite material and the solidifying cement mixture. Furthermore, CDF in CDF/DFNS filled smaller pores in the solidified cement mortar, thereby enhancing the density and improving the tangible efficiency of cement-based materials.

The enhanced effectiveness of DFNS–CDF in cement can be defined by its improved distribution and reduced clumping when compared to CDF. The pozzolanic activity noticed on the exterior of CDF is mainly linked with the active hydroxyl group and a lack of outward zone following ionization. However, after modification with DFNS, the existence of active points and defects on the exterior of CDF diminished, bringing about a slump in its competence to form C–S–H through the pozzolanic reaction. The tangible features displayed a decreasing pattern as the relation speed escalated. Fig. 15 illustrates the numerical link between compression capability and permeability, evaluating the filler effect brought about by CDF or CDF/DFNS on tangible strength. Notably, Fig. 15 organizes the permeability on the *x*-axis in a sequence from low to high. A negative power-law relation between permeability and pressure strength was noticed. As permeability rose, the pressure strength diminished. This effect was especially noticeable when the total permeability was in a lower gamut. This motif revealed that the reduction in total permeability positively influenced the strength of the pressure.

Previous research suggested that the main element affecting the imperishability of concrete in aquatic ecosystems is the dissolution induced by chloride ions.[31] This study was conducted to evaluate the resistance of cement mortar cases to Cl^- corrosion using the quick Cl^- diffusion coefficient technique. The Cl^- diffusion coefficient was assessed after a curing age of 21 days. The findings (Fig. 16) demonstrated changes in chloride movement index and intrusion extent for mortar cases with CDF and CDF/DFNS. These samples showed improved resistance to Cl^- corrosion compared to the control samples. The samples doped with DFNS–CDF revealed the smallest depth of infiltration chloride and the lowest diffusion coefficient of chloride; therefore, showing the highest efficiency in terms of resistance to decay induced by chloride ions.

The numerical relationship between the overall permeability and the chloride movement index is depicted in Fig. 17. It is apparent that a direct correlation existed between the total permeability and the diffusion coefficients of Cl^-. This implies that with an increase in overall permeability, there was a corresponding gradual rise in the coefficient of chloride ion migration. Given that the CDF particles did not chemically bind with chloride ions, the imperviousness of the cement case to chloride ion could be linked to the remarkable solidity of the case. This elucidates the link between decreased permeability and intensified resistance to erosion instigated by chloride ions. CDF cases revealed a significantly higher chloride diffusion coefficient compared to CDF/DFNS. The addition of CDF instigated a notable change, substantially diminishing the cement paste's liquescence and leading to a rise in the occurrence of pores and flaws in the scenario. This claim is corroborated by the MIP measurements.

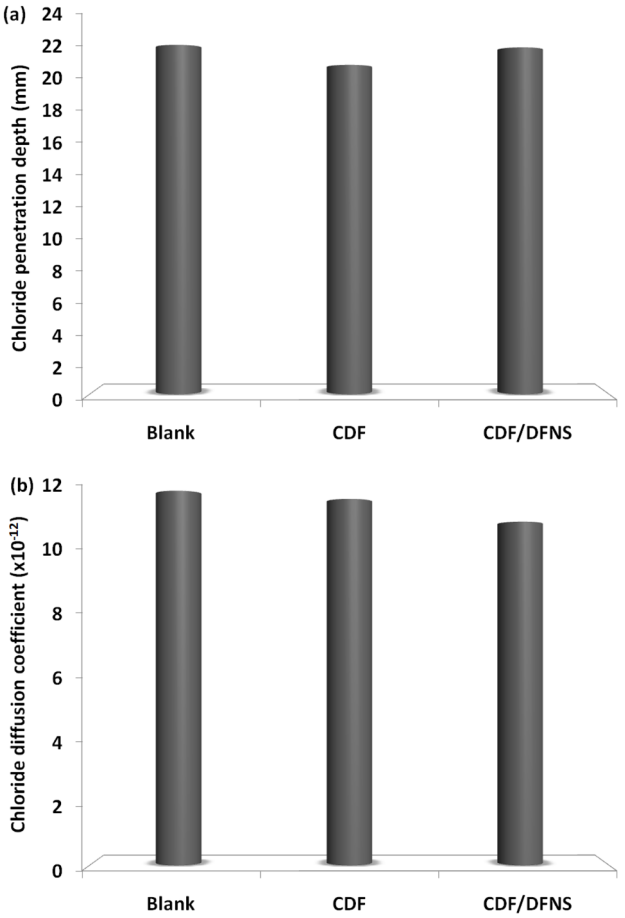

Fig. 16 Chloride penetration depth (a) and diffusion coefficient (b) at a 21-day rehabilitating age.

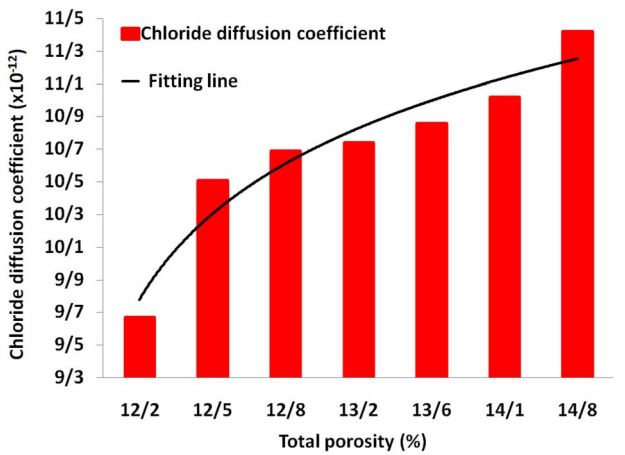

Fig. 17 The connection between overall permeability and the chloride diffusion coefficient at the restoration age of 21 days.

Conclusions

In the present study, CDF/DFNS was synthesized using cow dung fiber (CDF) and DFNS. The effects of CDF and CDF/DFNS on the flow attributes, chloride endurance, and internal arrangement of cement mortar were thoroughly evaluated. This was followed by an analysis of the fundamental mechanisms influencing these effects. The primary aim of this research was to determine the potential of using CDF and CDF/DFNS to boost the resilience and tangible strength of cement mortar. The results indicated that adding 2 wt% of CDF and CDF/DFNS could significantly reduce the permeability of cement mortar, while concurrently increasing its compressive strength and resistance to chloride penetration. This finding could potentially contribute to a strategy aimed at reducing CO_2 emissions.

Data availability

The data supporting the findings of this study are available within the article.

Conflicts of interest

There are no conflicts to declare.

Notes and references

1 R. Xiao, X. Jiang, Y. Wang, Q. He and B. S. Huang, *J. Mater. Civ. Eng.*, 2021, **33**, 04021312.
2 X. Jiang, R. Xiao, Y. T. Ma, M. M. Zhang, Y. Bai and B. S. Huang, *Constr. Build. Mater.*, 2020, **262**, 120579.
3 X. Jiang, R. Xiao, M. M. Zhang, W. Hu, Y. Bai and B. S. Huang, *Constr. Build. Mater.*, 2020, **254**, 119267.
4 K. K. Gupta, K. R. Aneja and D. Rana, *Bioresources and Bioprocessing*, 2016, **3**, 1–11.
5 U. Braun, *Veterinary Clinics of North America: Food Animal Practice*, 2016, **32**, 85–107.
6 S. S. Rath, D. S. Rao and B. K. Mishra, *Int. J. Miner. Process.*, 2016, **157**, 216–226.
7 S. K. Saraswat, M. Demir and V. Gosu, *Environmental Quality Management*, 2020, **30**, 51–60.
8 H. Bamogo, M. Ouedraogo, I. Sanou, K. A. J. Ouedraogo, K. Dao, J. E. Aubert and Y. Millogo, *Journal of Cultural Heritage*, 2020, **46**, 42–51.
9 L. Zhang and X. Sun, *Bioresour. Technol.*, 2017, **245**, 152–161.
10 C. M. Gong, *J. Environ. Sci.*, 2007, **19**, 1014–1019.
11 S. S. Rath, D. S. Rao and B. K. Mishra, *Int. J. Miner. Process.*, 2016, **157**, 216–226.
12 A. K. Yadav, K. Gaurav, R. Kishor and S. K. Suman, *International Journal of Pavement Research and Technology*, 2017, **10**, 254–261.
13 P. Vijayaraghavan, M. Kalaiyarasi and S. G. P. Vincent, *J. Genet. Eng. Biotechnol.*, 2015, **13**, 111–117.
14 W. Liao, Y. Liu, C. Liu and S. Chen, *Bioresour. Technol.*, 2004, **94**, 33–41.
15 K. L. Pickering, M. A. Efendy and T. M. Le, *Composites, Part A*, 2016, **83**, 98–112.
16 F. Ahmad, H. S. Choi and M. K. Park, *Macromol. Mater. Eng.*, 2015, **300**, 10–24.
17 M. S. Islam and S. J. Ahmed, *Constr. Build. Mater.*, 2018, **189**, 768–776.

18 H. Guo, Z. Wang, Q. Liang and G. Li, *Cem. Concr. Compos.*, 2022, **125**, 104330.
19 M. Khorami and E. Ganjian, *Constr. Build. Mater.*, 2011, **25**, 3661–3667.
20 G. H. D. Tonoli, M. N. Belgacem, G. Siqueira, J. Bras, H. Savastano Jr and F. R. Lahr, *Cem. Concr. Compos.*, 2013, **37**, 68–75.
21 R. Medeiros-Junior, M. Lima, P. Brito and M. H. F. D. Medeiros, *Ocean Eng.*, 2015, **103**, 78–87.
22 Y. Wang, X. Gong and L. Wu, *Constr. Build. Mater.*, 2019, **216**, 40–57.
23 W. Chalee, P. Ausapanit and C. Jaturapitakkul, *Mater. Des.*, 2010, **31**, 1242–1249.
24 X. Li, F. Rao, S. Song, S. X. Song and Q. Y. Ma, *J. Mater. Res. Technol.*, 2019, **8**, 2747–2752.
25 Y. Yi, D. J. Zhu, S. C. Guo, Z. H. Zhang and C. J. Shi, *Cem. Concr. Compos.*, 2020, **113**, 103695.
26 M. Z. Y. Ting, K. S. Wong, M. E. Rahman and M. S. Joo, *Constr. Build. Mater.*, 2020, **254**, 119195.
27 M. D. A. Thomas and J. D. Matthews, *Cem. Concr. Compos.*, 2004, **26**, 5–20.
28 M. Norouzi, M. Chafer and L. F. Cabeza, *Journal of Building Engineering*, 2021, **44**, 102704.
29 K. Xu, W. Huang, L. Zhang, S. Fu, M. Chen, S. Ding and B. Han, *Constr. Build. Mater.*, 2021, **287**, 123036.
30 J. Xu, Y. Li, L. Lu, X. Cheng and L. Li, *J. Cleaner Prod.*, 2023, **382**, 135281.
31 Y. Wang, X. Gong and L. Wu, *Constr. Build. Mater.*, 2019, **216**, 40–57.